Flexoelectricity and competition of time scales in electroconvection

Tibor Tóth-Katona, Nándor Éber, and Ágnes Buka
Research Institute for Solid State Physics and Optics, Hungarian Academy of Sciences, H-1525 Budapest, P.O. Box 49, Hungary

Alexei Krekhov
Physikalisches Institut, Universität Bayreuth, D-95440 Bayreuth, Germany

(Received 3 April 2008; revised manuscript received 31 July 2008; published 8 September 2008)

An unexpected type of behavior in electroconvection (EC) has been detected in nematic liquid crystals (NLCs) under the condition of comparable time scales of the director relaxation and the period of the driving ac voltage. The studied NLCs exhibit standard EC (s-EC) at the onset of the instability, except one compound in which nonstandard EC (ns-EC) has been detected. In the relevant frequency region, the threshold voltage for conductive s-EC bends down considerably, while for dielectric s-EC it bends up strongly with the decrease of the driving frequency. We show that inclusion of the flexoelectric effect into the theoretical description of conductive s-EC leads to quantitative agreement, while for dielectric s-EC a qualitative agreement is achieved. The frequency dependence of the threshold voltage for ns-EC strongly resembles that of the dielectric s-EC.

DOI: 10.1103/PhysRevE.78.036306 PACS number(s): 47.54.−r, 61.30.Gd, 47.20.Lz

I. INTRODUCTION

Electroconvection (EC) in nematic liquid crystals (NLCs) is an extensively studied example of electric field induced instabilities [1–3]. It also serves as a convenient model system for investigating pattern forming phenomena in complex, anisotropic fluids driven out of equilibrium.

NLCs have a uniaxial orientational order which is represented by the unit vector **n**, the director. Consequently, NLCs possess direction dependent physical properties. The dielectric anisotropy $\varepsilon_a=\varepsilon_\parallel-\varepsilon_\perp$ and the conductivity anisotropy $\sigma_a=\sigma_\parallel-\sigma_\perp$ are two key parameters in EC ($\parallel$ denotes the value along, and $\perp$ the value perpendicular to the director). While ε_a governs the electric torque acting on the director in the presence of electric fields, the director distortions lead to an elastic restoring torque exerted on **n**. Furthermore, the uniaxial symmetry of NLCs allows for a coupling between director orientation and flow, characterized by the five independent viscosity coefficients, resulting in a viscous torque if velocity gradients and/or temporal variation of **n** are present.

Electroconvection has most commonly been observed in planarly oriented (**n** parallel to the substrates) layers of nematics with $\varepsilon_a<0$ and $\sigma_a>0$, though it shows up at some other combinations of ε_a, σ_a and initial director orientation too [3]. In experiments usually samples of $10\ \mu\mathrm{m}\lesssim d\lesssim 100\ \mu$m thickness have been used. EC appears at a threshold rms value U_c of the applied ac voltage U of frequency f as a pattern consisting of dark and bright stripes with wave vector **q** when viewed in a microscope. EC patterns have great morphological richness at the onset: normal rolls (**q** parallel with the initial **n**) and oblique rolls (**q** encloses a finite angle with **n**), stationary as well as traveling patterns have been detected depending on material parameters and on the driving frequency.

Detailed theoretical studies in recent decades have established a firm understanding of this pattern forming phenomenon, combining the equations of nematohydrodynamics (anisotropic Navier-Stokes equation for the flow plus the balance of torques acting on the director) with those of electrodynamics assuming that the NLC has an Ohmic electrical conductivity. First it has been shown using a simple one-dimensional approximation that the EC pattern is excited by the Carr-Helfrich feedback mechanism [4,5]: spatial director modulations induce a separation of space charges due to the anisotropic conductivity; electrostatic forces induce a flow in the form of vortices; flow exerts a destabilizing viscous torque on the director against restoring elastic and electric torques. When this feedback becomes positive (at $U\geqslant U_c$) a specific director fluctuation grows up; i.e., a periodic director modulation, characterized by a finite tilt angle with respect to the initial alignment, develops. As the director is the optical axis of the NLC, the tilt leads to a modulation of the refractive indices. The pattern becomes optically detectable either with or without a polarizer due to light focusing or defocusing effects (shadowgraph image [6]) as well as via birefringence if crossed polarizers are used. The complex physical phenomena involved in the mechanism occur on three different time scales, characterized by the director relaxation time $\tau_d=\frac{\gamma_1 d^2}{K_{11}\pi^2}$, the charge relaxation time $\tau_q=\frac{\varepsilon_0\varepsilon_\perp}{\sigma_\perp}$, and the viscous relaxation time $\tau_v=\frac{\rho d^2}{\alpha_4/2}$. Here K_{11} is the splay elastic modulus, ρ is the density, γ_1 is the rotational, and $\alpha_4/2$ is the isotropic viscosity [7]. Typically $\tau_d\gg\tau_q\gg\tau_v$ [1]. For example, in a $d=20\ \mu$m sample of nematic Phase 5 (Merck & Co., Inc.) with a typical conductivity of $\sigma_\perp=8.2\times10^{-8}\ (\Omega\ \mathrm{m})^{-1}$ at $T=30\ ^\circ$C, one has $\tau_d=0.46$ s, $\tau_q=5.6\times10^{-4}$ s, and $\tau_v=1.4\times10^{-5}$ s.

Though the one-dimensional (1D) theoretical description managed to capture the essence of the instability mechanism, it represents a substantial simplification of the problem, therefore the applicability of the resulting (approximate) analytical formulas are limited. This has necessitated later the development of a comprehensive three-dimensional (3D) theory, composed of six coupled partial differential equations (PDEs), known today as the standard model (SM) of EC [8]. The equations can be conveniently made nondimensional by measuring lengths in units of d/π and time in units of τ_d. Then via a linear stability analysis the SM can provide the frequency dependence of the threshold voltage $U_c(f)$, that of the critical wave vector, as well as the spatiotemporal depen-

dence of the director, the velocity, and the charge density perturbations at onset. According to the model, a finite threshold of the primary instability in planar geometry requires a positive σ_a and a negative (or slightly positive) ε_a. Under these conditions, depending on the driving frequency f, two different solution types exist. Below the crossover frequency f_c, in the conductive regime, the charge distribution oscillates with f, while the director field is stationary in leading order. In this regime, SM gives two solutions with different spatiotemporal symmetry (mode I and mode II), however, for the threshold behavior only the solution with the lower U_c (mode I) is relevant [9,10]. Above f_c, in the dielectric regime, the situation is reversed: the charge distribution is stationary in leading order, while the director oscillates with f. Here, the model also yields two solutions (mode III and mode IV), but the threshold behavior is described by mode III which has lower U_c compared to mode IV. Modes I–IV are graphically presented in Fig. 1(a) of Ref. [9], while the spatiotemporal symmetries of the field variables for these modes are summarized in Table I of Ref. [11]. These electroconvection scenarios that are captured by the SM, will be referred to as standard electroconvection (s-EC). Various predictions of the SM have been compared with experimental results obtained on a number of NLCs and usually an excellent agreement has been found—see, e.g., [2,12,13].

In s-EC, the conductive and the dielectric regimes correspond to two competing pattern forming modes which have different $U_c(f)$ and $U_c(d)$ characteristics. The frequency dependence of U_c and q_c has a concave (diverging) shape in the conductive regime whereas they have a square-root-like behavior in the dielectric one. As far as the thickness dependence is concerned, an inspection of the nondimensional equations of the SM shows that by scaling only five of the six PDEs became invariant with respect to d; the equation for the induced potential still has an explicit d dependence via a factor $\tau_d/\tau_q \propto \sigma_\perp d^2$—see e.g., Eqs. (A6)–(A11) in [11]. Nevertheless, in the conductive regime, U_c is thickness independent in the lowest order time Fourier approximation for the experimentally most relevant (10–100 μm) thickness range, where $\tau_d \gg \tau_q$ [8]. In contrast, in the dielectric regime an analogous approximation gives $U_c \propto d$.

At typical ($d \geqslant 10$ μm) cell thicknesses the conductive regime appears at low frequencies and the dielectric rolls are observable at higher f. The change of pattern type occurs at f_c, which depends significantly on $\sigma_\perp$ as well as on d. Therefore, in order to extend the frequency range of the dielectric regime, thus to shift f_c to lower values, one has to reduce either the cell thickness or the electric conductivity or both. When both $\sigma_\perp$ and d are small enough, the conductive regime does not occur at all.

What has been said above, applies not only to substances with material parameters satisfying $\varepsilon_a<0$, $\sigma_a>0$, but also for $\varepsilon_a>0$, $\sigma_a<0$ with the appropriate boundary conditions [3]. In contrary, in the case of nematics with $\varepsilon_a<0$ and $\sigma_a<0$ [3,14], where the feedback loop remains negative for all voltages, the Carr-Helfrich mechanism excludes the existence of EC patterns. Nonetheless, a convection roll pattern has long ago been observed in such compounds in ac electric field [15,16] and has been reconsidered systematically recently in a few nematics [17–19]. Some basic characteristics of these patterns, such as the orientation of the rolls (nearly parallel with the initial **n**), the contrast, the frequency dependence of U_c, and that of the critical wave number, have been found considerably different from those of the s-EC. Since this kind of pattern formation is not predicted by the SM, it has been called nonstandard electroconvection (ns-EC) [17]. Recently, convection patterns with similar properties have been detected in nematics built up from bent-core molecules [20–22] that may exhibit giant flexoelectricity [23].

The SM regards NLCs as regular dielectrics, where the source of the electric polarization is the electric field. In NLCs, however, flexoelectric polarization [24,14,25] may appear even in the absence of the electric field, if the director field is distorted. Flexoelectricity produces an additional contribution to the charge distribution and to the electric torque acting on the director. It is also known for a long time that under large enough dc voltage, flexoelectricity may distort the director field in the planar geometry resulting in a nonconvective striped pattern oriented parallel with the initial **n** [26]. The threshold voltage and the wave number of this nonconvective pattern, as well as the frequency dependence of the threshold characteristics have been calculated [27] and measured for dc excitation [28].

Earlier studies on the effect of flexoelectricity on EC have shown that for the commonly used nematic material parameters, and for a typical sample thickness of $d \gtrsim 10$ μm, in the usually studied (not too low) frequency range of conductive s-EC, flexoelectricity has no significant influence on the characteristics at the onset of instability [29–31]. That gives the reason why the contribution of the flexoelectric polarization has been neglected in the SM. On the other hand, it has also been shown that when applying a dc voltage, the EC threshold becomes independent of d and $\sigma_\perp$ [29]. Moreover, flexoelectricity leads to an appreciable reduction of the dc EC threshold and it also influences the direction of the rolls [30]. Obviously, there must be an ac frequency range in which the effect of flexoelectricity diminishes with the increase of the frequency. This frequency range, however, has not yet been studied in detail.

If flexoelectricity is included into the SM (furthermore referred to as *extended* SM), two additional parameters, the flexoelectric coefficients e_1 and e_3 [24] (more precisely, their combinations e_1-e_3 and e_1+e_3 [9]) come into play. An analysis of the nematohydrodynamic equations linearized around the basic state has proven that flexoelectricity establishes a coupling between the conductive and dielectric modes introduced above [9,11] resulting in a complex time dependence. The solutions still can be classified according to their spatiotemporal parity [11]. The even parity solution has mode I coupled to mode IV (mode I+IV), and corresponds to the "conductive regime," while in the odd parity "dielectric" solution mode III couples to mode II (mode II+III) [32].

Experiments on ns-EC have triggered a recent reconsideration of the role of flexoelectricity within the extended SM for a wider range of material parameters. It has been shown that in some cases flexoelectricity cannot be disregarded. At high frequencies, in the dielectric regime a nonzero e_1 and e_3 leads to a considerable decrease of U_c [33]. What is even more important, the flexoelectric contribution to the charge

separation yields finite instability threshold for planar nematics with $\sigma_a<0$ and $\varepsilon_a<0$, thus giving an explanation for ns-EC [11].

Special behavior can be expected (some might go beyond the applicability limit of the SM) in the parameter ranges where the period of the driving frequency $1/f$ becomes comparable with one of the characteristic times of the system τ_d, τ_q, or τ_v. The majority of the experimental and theoretical studies of EC so far apply to relatively thick cells ($d \geqslant 10\ \mu$m) of medium conductivity [$\sim 10^{-8}\ (\Omega\ \mathrm{m})^{-1}$], thus they do not extend to this range. We aim to fill this gap and we also show that flexoelectricity plays a crucial role in those ranges.

In the present paper we report on experimental studies and numerical simulations of EC aiming to approach the characteristic times of the system by $1/f$, especially concentrating on τ_d and in some special cases on τ_q (τ_v is usually very short; to approach it would require very thick cells and high driving frequencies, which would result in high threshold voltages not accessible experimentally). We focus on the frequency dependence of the threshold voltage $U_c(f)$. The measurements have been carried out on five different nematic compounds: four of them exhibit s-EC, while in the fifth one, both s-EC and ns-EC patterns could be observed. The numerical analysis has been based on the extended standard model of EC which includes the flexoelectric effects [9,11].

The structure of the paper is organized according to the pattern type in the low frequency range. After introducing the substances, the setup, and some details of the numerical analysis in Sec. II, Sec. III is devoted to results on compounds in which conductive s-EC has been detected at low frequencies. In Sec. IV we discuss samples which exhibit dielectric s-EC at low f, while Sec. V describes the ns-EC instability. Finally, we conclude the paper with the Discussion in Sec. VI.

II. SUBSTANCES, EXPERIMENTAL SETUP, AND DETAILS OF CALCULATIONS

Five different NLCs have been used in the measurements. The three commercial nematic mixtures, Phase 5, Phase 5A, and Phase 4 (from Merck & Co., Inc.) as well as the 4-methoxy-benzylidene-4′-*n*-butyl-aniline (MBBA) have $\sigma_a>0$ and $\varepsilon_a<0$; so they exhibit s-EC upon application of an electric voltage. All measurements presented here on these compounds have been performed at $T=30\ ^\circ$C.

The fifth studied compound was the 4-*n*-octyloxy-phenyl-4-*n*′-heptyloxy-benzoate (**8**/**7**) [34] which has the phase sequence: isotropic–92 °C–nematic–72.5 °C–smectic C–62 °C–crystalline. It has $\varepsilon_a<0$ over the whole nematic temperature range, but shows a sign inversion from $\sigma_a<0$ to $\sigma_a>0$ as the temperature is increased toward the clearing point. Consequently, in this particular compound both ns-EC and s-EC could be investigated (although at different temperatures).

Our aim is to study the EC onset behavior in the vicinity of the characteristic relaxation times of the system; in order to approach that we have varied the cell thickness and the conductivity to tune τ_d and τ_q.

The nematic liquid crystals have been enclosed between two parallel glass plates coated with etched transparent indium tin oxide (ITO) electrodes. Rubbed polyimide has been used to obtain a planar alignment. Cells in the thickness range from $d\approx 3\ \mu$m to $d=40\ \mu$m have been prepared. A spectrophotometer has been used for measuring d. It also enabled a systematic mapping of the thickness of the empty cell, thus determining its total variation throughout the whole active area (region between electrodes) of the sample. Typically, we have found a variation of $\pm 0.5\ \mu$m. The conductivity range extended from $10^{-9}\ (\Omega\ \mathrm{m})^{-1}$ to $10^{-7}\ (\Omega\ \mathrm{m})^{-1}$. The direction of the director at the surfaces is chosen as the x axis. An electric field across the sample (along the z axis) has been generated by applying a sinusoidal ac electric voltage of frequency f and amplitude $\sqrt{2}U$ to the electrodes. The cells have been placed into an oven (an Instec hot stage) thermostatted within $\pm 0.05\ ^\circ$C.

EC patterns have been studied with polarizing microscopy using either the shadowgraph (single polarizer) technique or two crossed (or nearly crossed) polarizers. The images have been recorded with a video camera, digitized by a frame grabber with a resolution of at least 768×576 pixels and 24 bit color depth and saved for further processing and analysis.

Numerical simulations have aimed to compute the frequency dependent threshold voltage $U_c(f)$ for the different EC patterns. The extended SM (with flexoelectricity included) has been used. Being interested in the onset behavior, linear stability analysis has been carried out as described in detail in [11]. Strong anchoring of the director and no-slip condition for the flow have been assumed at the bounding plates, which have been ensured by a Galerkin method [35]. The field variables have been expanded into sets of functions that vanish at the boundaries; the time periodicity has been guaranteed by Fourier expansion. Expansions in space and time have been truncated at the fourth and the seventh modes, respectively, which has been proved sufficient to obtain accuracy of better than 1% in $U_c(f)$. This has been checked at the low and high frequency limits by increasing systematically the number of modes in space and time up to 10 and 15, respectively, and monitoring the changes in U_c. The growth rates $\mu(\mathbf{q},U)$ for spatial fluctuations have been calculated as a function of the applied voltage. The minimum of the neutral surface $[\mu(\mathbf{q},U)=0]$ provided the threshold voltage U_c. The numerical calculations have been carried out with a Fortran code developed at the University of Bayreuth, using the same set of known material parameters (permittivities, conductivities, elastic moduli, viscosities), as for earlier calculations with the SM (for Phase 5 and Phase 5A in [36], and for MBBA in [8,37,38]). The original measurements of these parameters have been reported in [36,39,40] for Phase 5 and in [41–46] for MBBA.

The splay and bend flexoelectric coefficients, e_1 and e_3, should also be known, however, they are not easily measurable. Though various measuring techniques have been developed during recent decades, there is still a big controversy about the value and the sign of e_1 and e_3. The data obtained by different methods vary considerably even for the most studied nematic material, MBBA: e_1+e_3 ranges from -2.3 pC/m [47] to $-(54\pm 10)$ pC/m [48], and e_1-e_3 from

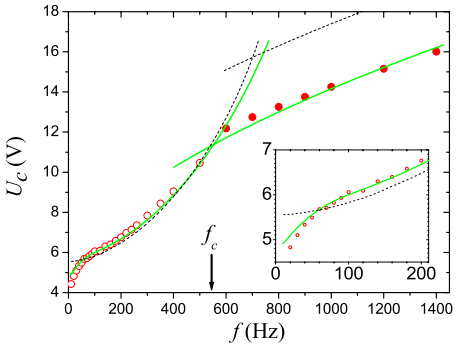

FIG. 1. (Color online) Frequency dependence of the s-EC threshold voltage U_c measured in Phase 5 with $d=(3.4\pm0.5)$ μm—conductive s-EC (circles) and dielectric s-EC (bullets). The solid and the dashed lines are the results of the numerical analysis with and without the flexoelectric effect, respectively. The inset is the magnification of the low frequency range. The arrow indicates the crossover frequency f_c.

(3.3 ± 0.7) pC/m [49] to (14 ± 1) pC/m [48]. Up to now, only the sign of the sum of flexoelectric coefficients seems to be above dispute for MBBA: it appears to be negative ($e_1+e_3<0$). For the other four compounds used in our experiments no data on the flexoelectric coefficients are at all currently available. It seems though, based on measurements on a number of (other) nematics, that at least the order of magnitude of ~10 pC/m is established as a customary value for both e_1 and e_3 [50]. As a consequence, during the numerical simulations we have regarded e_1 and e_3 as adjustable parameters, to be chosen to provide the best fit with the experiments.

III. CONDUCTIVE s-EC AT LOW FREQUENCIES AND DIELECTRIC s-EC AT HIGH FREQUENCIES

We start the discussion of the experimental results with systems exhibiting s-EC, where by choosing d and $\sigma_\perp$ appropriately, the frequency range of the ac field covers $1/\tau_d$ and in most cases $1/\tau_q$ as well. The first case we show is electroconvection in Phase 5 with $d=(3.4\pm0.5)$ μm and $\sigma_\perp=8.2\times10^{-8}$ $(\Omega\,\mathrm{m})^{-1}$. In this case $1/\tau_d\approx60$ Hz, $1/\tau_q\approx1800$ Hz, and $1/\tau_v\approx2\times10^6$ Hz.

Threshold measurements are presented in Fig. 1. Below $f_c\approx550$ Hz conductive s-EC (open circles) has been detected at onset in the form of traveling oblique rolls and traveling normal rolls. Above f_c traveling dielectric s-EC (bullets) has been observed.

An unexpected feature of the $U_c(f)$ curve has been detected in the low frequency range, 20 Hz$\lesssim f\lesssim$60 Hz, where the threshold strongly decreases by lowering the frequency, in contrast to thick ($d\geqslant10$ μm) cells where U_c remains almost constant in the same frequency range.

Numerical calculations have been performed with the Phase 5 parameter set (see Table I), using the flexoelectric coefficients e_1 and e_3 as fitting parameters. In Fig. 1 the results are plotted both without the flexoelectric effect ($e_1=e_3=0$, dashed lines, representing mode I and mode III) and with flexoelectric coefficients of $e_1=-26.5$ pC/m and $e_3=-23.6$ pC/m (solid lines, mode I+IV and mode II+III). For the conductive s-EC, the calculation without the flexoelectric effect does not show the bending down at low frequencies, while with the e_1 and e_3 values given above, a good match with the experimental data has been obtained both for the conductive and the dielectric regimes (see the two curves in the inset of Fig. 1).

TABLE I. Material parameters of Phase 5 and MBBA at $T=30$ °C. Phase 5 parameters have also been used in numerical calculations for Phase 5A.

Parameter	Unit	Phase 5	MBBA
K_{11}	10^{-12} N	9.8 [36]	5.89 [41]
K_{22}	10^{-12} N	4.6 [36]	3.7 [41]
K_{33}	10^{-12} N	12.7 [36]	7.56 [41]
$\sigma_a/\sigma_\perp$		0.69 [36]	0.5 [42]
$\varepsilon_\perp$		5.25 [36]	5.18 [42]
ε_a		−0.184 [36,39]	−0.48 [42]
α_1	10^{-3} N s/m^2	−39 [36]	−14.1 [45]
α_2	10^{-3} N s/m^2	−109.3 [40]	−80.0 [45]
α_3	10^{-3} N s/m^2	1.5 [40]	−1.513 [45]
α_4	10^{-3} N s/m^2	56.3 [40]	64.4 [45]
α_5	10^{-3} N s/m^2	82.9 [40]	57.2 [45]
α_6	10^{-3} N s/m^2	−24.9 [40]	−24.4 [45]
e_1	pC/m	−26.5 (fit)	−14.5 (fit)
e_3	pC/m	−23.6 (fit)	−20.5 (fit)

Calculations have been performed for a $d=20$ μm cell as well, using the same parameters from Table I and $\sigma_\perp=8.2\times10^{-8}$ $(\Omega\,\mathrm{m})^{-1}$ (providing $1/\tau_d\approx2$ Hz, $1/\tau_q\approx1800$ Hz, and $1/\tau_v\approx70\times10^3$ Hz). The results are plotted in Fig. 2. One can immediately see that the resulting $U_c(f)$ for $e_1=e_3=0$ (mode I) nearly coincides with the one incorporating the flexoelectric effect (mode I+IV) almost in the whole conductive frequency range, in accordance with earlier conclusions [29]. Nevertheless a closer look at the curves (see the inset of

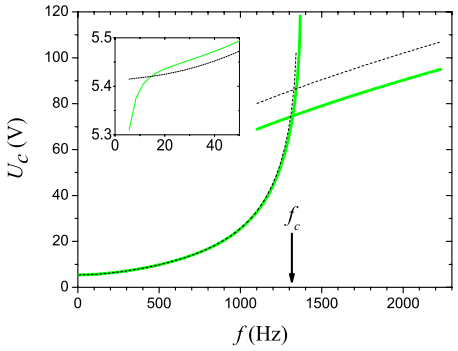

FIG. 2. (Color online) Numerical calculations for the frequency dependence of the s-EC threshold voltage U_c in a $d=20$ μm sample of Phase 5 with $\sigma_\perp=8.2\times10^{-8}$ $(\Omega\,\mathrm{m})^{-1}$. Dashed lines are the conductive s-EC and the dielectric s-EC solutions with $e_1=e_3=0$, while the solid lines are the solutions with $e_1=-26.5$ pC/m and $e_3=-23.6$ pC/m. The inset is the magnification of the low frequency range. The arrow indicates the crossover frequency f_c.

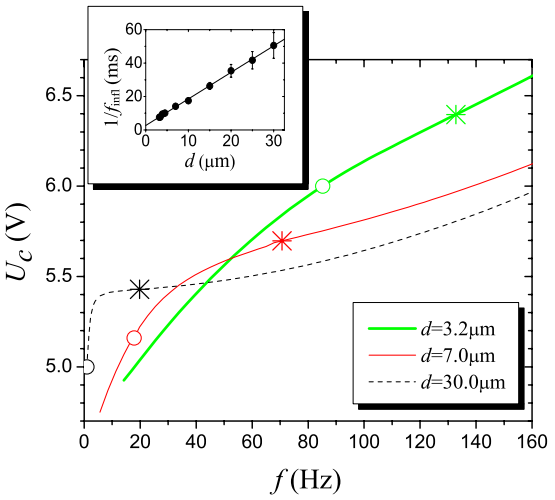

FIG. 3. (Color online) Numerically calculated frequency dependence of the s-EC threshold voltage U_c for samples of various thicknesses in Phase 5 with $\sigma_\perp = 8.2 \times 10^{-8}$ $(\Omega\,\mathrm{m})^{-1}$, $e_1 = -26.5$ pC/m, and $e_3 = -23.6$ pC/m. The circles and the star symbols on the curves denote $1/\tau_d$ and the inflection point at f_{infl}, respectively. Inset: the thickness dependence of $1/f_{\mathrm{infl}}$.

Fig. 2 with a blowup of the plot) shows that switching on the flexoelectricity results in the bending down of the threshold here too, similarly to the case of low d, only the effect occurs here at much lower frequencies.

The bending down of U_c at low f when flexoelectricity is included can be understood from the earlier theoretical results [30] where it has been shown that flexoelectricity decreases the dc threshold voltage considerably (for MBBA the reduction is about 25%). It could also be proved that in this dc limit none of the dimensionless equations of SM depend on $\sigma_\perp d^2$, hence the dc threshold is independent of d and $\sigma_\perp$ [29]. In the case of ac driving there is a wide frequency range (in the middle of the conductive regime) where flexoelectricity has much less influence on U_c; it leaves the ac threshold almost unaltered, at least for not too thin cells. This means that at increasing f the contribution from the flexoelectric charge separation (important at dc) fades away compared to that of the Coulomb charge density in a narrow frequency range at low f. The character of this transition from dc to ac driving has, however, not been studied rigorously either experimentally or theoretically so far.

In order to understand better the behavior of U_c we have carried out further simulations, carefully analyzing the low frequency range for a series of thicknesses when flexoelectricity is included. Results are shown in Fig. 3 for three thicknesses. The figure indicates that the transition from ac to dc (the bending down of U_c to its dc value) occurs for any thickness as expected; only the effect is compressed into a very narrow frequency range for large thicknesses. The corresponding values of $1/\tau_d$ are also indicated in Fig. 3 (circles). Their values fall into those frequency ranges (different for each d) in which the strong bending down of U_c occurs. We note, that according to its definition, τ_d is the relaxation time of a homogeneously deformed director state (wave number $|\mathbf{q}|=0$). The relaxation time of the pattern, $1/\tau_p$, is shorter, because the growth or decay rate ($\mu = 1/\tau_p$) of a periodic ($|\mathbf{q}| \neq 0$) distortion increases with $|\mathbf{q}|$ [51,52]. Therefore $1/\tau_p > 1/\tau_d$ would be a more appropriate characteristic frequency of the system than $1/\tau_d$. A rigorous quantitative comparison of $1/\tau_p$ with f is, however, problematic since $|\mathbf{q}|$ and hence τ_p are frequency dependent.

The crossover between the regimes where the Coulomb charge separation or the flexoelectric charge separation dominates, is reflected in the curvature of the $U_c(f)$ curves. It is convenient to use the location of the inflection point at f_{infl} (where the curvature changes sign, indicated by stars in Fig. 3) as a quantitative measure. As one can see, values of f_{infl} are close to $1/\tau_d$, but interestingly, $1/f_{\mathrm{infl}}$ is linear with d (see the inset of Fig. 3), in contrast to the d^2 dependence of τ_d.

Finally, we mention that for the high frequency end of the conductive regime the influence of flexoelectricity again becomes noticeable though less dramatic. It considerably enhances the d dependence (see Fig. 3) which would be almost negligible at $e_1 = e_3 = 0$, especially for higher thicknesses. Furthermore, it shifts f_c to lower frequencies as seen in Fig. 1.

The shift of f_c is mainly due to the fact that in the dielectric regime of s-EC the flexoelectric effect decreases the threshold voltage drastically—compare the dashed curve ($e_1 = e_3 = 0$, mode III) and the solid line ($e_1 = -26.5$ pC/m and $e_3 = -23.6$ pC/m, mode II+III) for the dielectric solutions above f_c in Figs. 1 and 2. The reduction reaches about 16% even in the relatively thick ($d = 20$ μm) sample, which agrees with recent findings for MBBA [33]. Consequently, flexoelectric effects cannot be neglected in case of dielectric s-EC even in the thick samples. We also mention here that no peculiar effect on $U_c(f)$ is observed in the vicinity of $1/\tau_q \approx 1800$ Hz (see Fig. 2).

Summarizing the results above, one can conclude that with the above mentioned values of $\sigma_\perp$, e_1, and e_3, an excellent agreement has been found between the experimental results (symbols) and the numerical calculations (solid lines in Fig. 1) for Phase 5 in the whole experimentally covered frequency range. Note that the fitted e_1 and e_3 values are realistic in a sense that they are of the same order of magnitude as those measured for other nematics.

Similar results have also been obtained on Phase 5A and MBBA samples in which only the conductive regime of s-EC has been detected. Phase 5A has been investigated in a sample of $d = 3.1$ μm. At dc voltage as well as at very low frequencies (up to $f \approx 3$ Hz) static stripe patterns, the so-called flexoelectric domains [27,53], have been observed at a threshold U_f. Above $f = 3$ Hz only conductive s-EC patterns have been seen: up to $f = 40$ Hz stationary oblique rolls and above $f = 40$ Hz traveling oblique rolls and traveling normal rolls. The measured frequency dependence of the threshold voltage is presented in Fig. 4 by open circles. Below $f \approx 50$ Hz it appears that U_c decreases considerably as approaching $f = 0$ (see the inset in Fig. 4), in a similar fashion as seen for the Phase 5 in Fig. 1. Again the bending down occurs in the frequency range of $1/\tau_d$.

Phase 5A has the same chemical composition as Phase 5 except that Phase 5A is doped with some ionic salt in order to increase the electric conductivity. Therefore, in the numerical calculations for Phase 5A we have used the material parameters of Phase 5 (given in Table I) with $\sigma_\perp = 9.2$

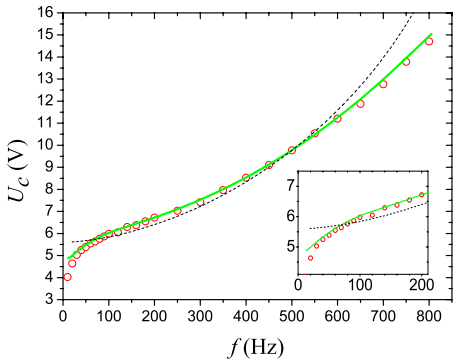

FIG. 4. (Color online) Frequency dependence of the threshold voltage U_c in the conductive regime for a sample of Phase 5A with $d=3.1$ μm. Circles stand for experimental data. The solid line represents the $U_c(f)$ curve calculated numerically with Phase 5 parameters (the same as in Fig. 1, with nonzero e_1 and e_3) and with $\sigma_\perp = 9.2\times10^{-8}$ $(\Omega\,\mathrm{m})^{-1}$. The dashed line is the calculated solution for $e_1=e_3=0$. The inset is the magnification of the low frequency range.

$\times10^{-8}$ $(\Omega\,\mathrm{m})^{-1}$, and the flexoelectric coefficients $e_1=-26.5$ pC/m and $e_3=-23.6$ pC/m that have been obtained from the best fit in Fig. 1. The calculated threshold curve for conductive s-EC (solid line in Fig. 4) agrees very well with the experimental data in the whole frequency range.

For reference, in Fig. 4 we have also plotted the conductive s-EC threshold $U_c(f)$ without the flexoelectric effect (i.e., for $e_1=e_3=0$; dashed line). The same conclusions can be drawn here as those for Phase 5: the $U_c(f)$ curve with $e_1=e_3=0$ deviates significantly and systematically from that with nonzero e_1 and e_3 (and also from the experimental data), especially in the low frequency range (below $f\approx50$ Hz) and at high frequencies (above 600 Hz).

Up to now the most studied nematic EC material is presumably MBBA which we have investigated too, in a cell of $d=3.2$ μm. At dc voltage neither flexoelectric domains, nor periodic EC patterns have been detected up to $U=80$ V. However, at and above $f=0.1$ Hz a conductive s-EC pattern has emerged. Frequency dependence of the threshold voltage measured in this thin layer of MBBA is shown in Fig. 5 (circles). Again, below $f\approx30$ Hz $U_c(f)$ bends down considerably while approaching $f\to0$, in a similar fashion as seen for Phase 5 and Phase 5A.

The MBBA parameter set from Table I has been used in the numerical calculations. The solid line in Fig. 5 obtained by the simulations for $e_1=-14.5$ pC/m, $e_3=-20.5$ pC/m, and $\sigma_\perp=9\times10^{-8}$ $(\Omega\,\mathrm{m})^{-1}$ represents a fairly good match with the experimental data, in contrast to the curve with $e_1=e_3=0$ (dashed line in Fig. 5) which deviates significantly. One has to note here that the fitted values of e_1 and e_3 fall in the midrange of measured values for MBBA [50], and in particular agree reasonably well with the values $|e_1|=15$ pC/m and $|e_3|=30$ pC/m reported in [54,55].

IV. DIELECTRIC s-EC AT LOW FREQUENCIES

With a careful preparation procedure we were able to produce thin ($d=3.4$ μm) Phase 5 samples with a conductivity as low as about $\sigma_\perp\approx1\times10^{-8}$ $(\Omega\,\mathrm{m})^{-1}$. These samples exhibited convection-free flexoelectric domains at a threshold U_f at dc and at very low frequency (up to $f=7.5$ Hz) ac driving, similarly to the situation in Phase 5A. Above $f=7.5$ Hz, in a narrow frequency range (up to $f\approx20$ Hz) flexoelectric domains and traveling dielectric s-EC oblique rolls coexist with slightly different thresholds. At higher frequencies dielectric s-EC could be detected in the form of traveling oblique, or traveling normal rolls.

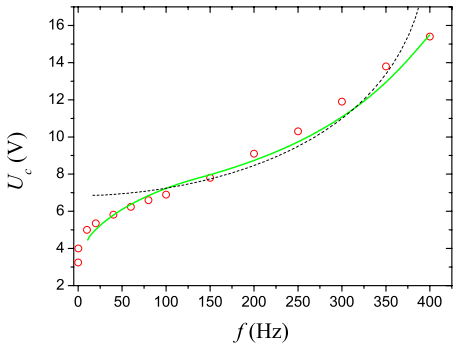

FIG. 5. (Color online) Frequency dependence of the conductive s-EC threshold voltage U_c measured on a sample of MBBA with $d=3.2$ μm (circles). The solid line represents the $U_c(f)$ curve calculated numerically with MBBA parameters from Table I and with $\sigma_\perp=9\times10^{-8}$ $(\Omega\,\mathrm{m})^{-1}$, $e_1=-14.5$ pC/m, and $e_3=-20.5$ pC/m. The dashed line is the solution for the same parameter set, but with $e_1=e_3=0$.

The frequency dependence of U_c in this sample (depicted with bullets in Fig. 6) is, however, rather unusual and surprising, considering that both the SM and previous experiments on dielectric s-EC provided a square-root-like $U_c(f)$ function. Instead, here $U_c(f)$ bends up as $f\to0$, i.e., it is a nonmonotonic function with an expressed minimum at $f_{\min}$ in the frequency range of $1/\tau_d$. Moreover, at higher frequencies (above the minimum) $U_c(f)$ is linear within the experimental error. Performing numerical simulations with the Phase 5 parameter set in Table I and with $\sigma_\perp=1\times10^{-8}$ $(\Omega\,\mathrm{m})^{-1}$, we have found that the calculated dielectric threshold curve $U_c(f)$ (shown as the solid line with the lowest U_c in Fig. 6) is monotonic, has a smaller slope (above 60 Hz), and provides lower thresholds (especially at high f) than found experimentally.

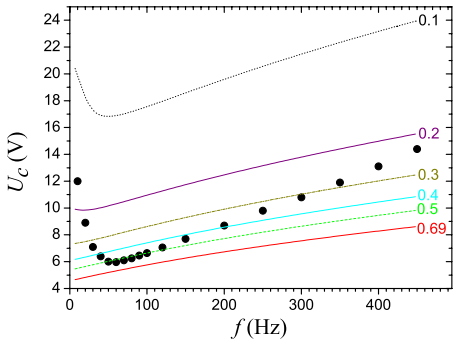

FIG. 6. (Color online) Frequency dependence of the dielectric threshold voltage U_c measured in a $d=3.4$ μm sample of Phase 5 (bullets). Lines represent results of numerical calculations for Phase 5 with $e_1=-26.5$ pC/m, $e_3=-23.6$ pC/m, and $\sigma_\perp=1\times10^{-8}$ $(\Omega\,\mathrm{m})^{-1}$ for a series of $\sigma_a/\sigma_\perp$ values as indicated.

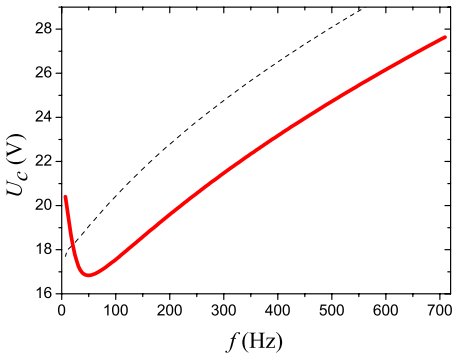

FIG. 7. (Color online) Numerical calculations of the threshold $U_c(f)$ for Phase 5 with $\sigma_a/\sigma_\perp=0.1$, $\sigma_\perp=1\times10^{-8}$ $(\Omega\,\mathrm{m})^{-1}$, and $d=3.4$ μm: the dashed line is dielectric s-EC with $e_1=e_3=0$; the solid line is the dielectric mode with $e_1=-26.5$ pC/m, $e_3=-23.6$ pC/m.

In order to test whether the extended SM is *able* at all to provide a $U_c(f)$ dependence with at least a *qualitative* similarity to the measured data, we have performed simulation experiments. First we have checked the influence of the conductivity systematically in a wide range of 10^{-12} $(\Omega\,\mathrm{m})^{-1}\leqslant\sigma_\perp\leqslant10^{-8}$ $(\Omega\,\mathrm{m})^{-1}$, where only dielectric s-EC is expected. We could verify that the calculated $U_c(f)$ remains monotonic in this $\sigma_\perp$ range, and dU_c/df is not affected significantly. Consequently, the experimental frequency dependence of the threshold (bending up) cannot be interpreted by a pure reduction of the conductivity.

We have also varied the anisotropy of the conductivity motivated by recent numerical results [11] indicating that a decrease of $\sigma_a/\sigma_\perp$ increases the slope dU_c/df and tends to make $U_c(f)$ linear. In Fig. 6 we present the calculated threshold curves for five additional $\sigma_a/\sigma_\perp$ values, leaving all other parameters in Table I unaltered. It is seen that $U_c(f)$ as well as dU_c/df shift to higher values with the decrease of $\sigma_a/\sigma_\perp$, moreover, $U_c(f)$ becomes nonmonotonic for $\sigma_a/\sigma_\perp\leqslant0.2$ with a bending up of $U_c(f)$ at low frequencies. Note that the curve calculated for $\sigma_a/\sigma_\perp=0.1$ reproduces qualitatively all features of the experimental $U_c(f)$, except that it is shifted to higher voltages.

To demonstrate the role of flexoelectricity in the novel frequency dependence of the dielectric regime, in Fig. 7 we have plotted $U_c(f)$ calculated with $\sigma_a/\sigma_\perp=0.1$ both for mode III (i.e., without flexoelectricity, dashed line) and for mode II+III (i.e., with flexoelectricity, solid line). Obviously, when flexoelectric effects are neglected, the threshold is even higher, $U_c(f)$ decreases monotonously when $f\to0$ and the bending up is not reproduced, so there is no agreement with the experimental data even on a qualitative level. On the other hand, if one takes into account the flexoelectric coefficients given in Table I, an acceptable qualitative agreement is achieved: the curve has a minimum at about the same $f_{\min}$ frequency where the experimental data, and for $f>f_{\min}$ the steepness dU_c/df is roughly the same as that in the experiments. Therefore, the bending up can undoubtedly be attributed to flexoelectricity, and $f_{\min}$ is a natural indicator for the frequency range where the crossover between dominantly flexoelectric and dominantly Coulomb charge separation mechanisms occur.

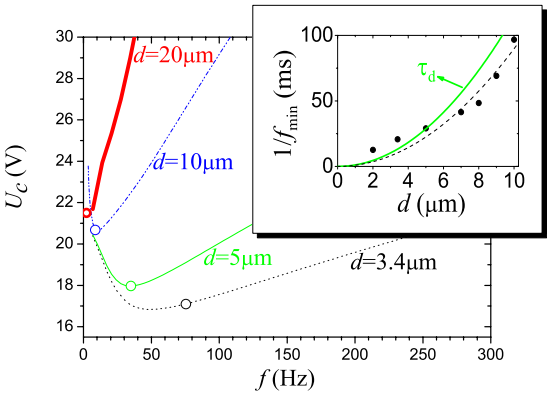

FIG. 8. (Color online) Frequency dependence of the dielectric s-EC threshold, calculated with Phase 5 parameters for $\sigma_a/\sigma_\perp=0.1$ and with $e_1=-26.5$ pC/m, $e_3=-23.6$ pC/m, $\sigma_\perp=1\times10^{-8}$ $(\Omega\,\mathrm{m})^{-1}$ for different sample thicknesses d as indicated. Circles denote $1/\tau_d$ for each d. In the inset the thickness dependence of $1/f_{\min}$ (bullets) and that of τ_d (solid line) is presented together with the best fit $1/f_{\min}\propto d^2$ (dashed line).

Finally, we mention that (similarly to the case discussed for Fig. 2) no peculiar effect of flexoelectricity on $U_c(f)$ is observed in the vicinity of $1/\tau_q\approx220$ Hz (see Figs. 6 and 7).

Systematic numerical calculations at $\sigma_a/\sigma_\perp=0.1$ have shown that while keeping $\sigma_\perp$ (and thus τ_q) constant, $f_{\min}$ shifts to higher f with the decrease of d (i.e., of τ_d)—see Fig. 8. Despite the fact that $1/f_{\min}$ increases linearly with d up to $d=8$ μm (similarly to $1/f_{\mathrm{infl}}$ of conductive s-EC), one finds the values of $1/f_{\min}(d)$ close to $\tau_d(d)$, and the best fit $1/f_{\min}\propto d^2$ does not differ significantly from $\tau_d(d)$ (see the inset of Fig. 8). At $d=20$ μm $U_c(f)$ becomes a monotonically increasing function (at least above $f=5$ Hz). One has to mention here that in our calculations we have not resolved the very low frequency range (~1 Hz), where the theoretical analysis becomes more difficult due to numerical problems and the experiments also require special care (and are, therefore, typically avoided). From Fig. 8 one also sees that the steepness of $U_c(f)$ in the high frequency range (where the function is close to linear) also depends on d; dU_c/df increases with d.

The other situation is when τ_q is tuned via $\sigma_\perp$ while keeping d and thus τ_d constant ($1/\tau_d=75.5$ Hz). The influence of $\sigma_\perp$ on $U_c(f)$ is illustrated in Fig. 9. With the increase of the conductivity (i.e., of $1/\tau_q$), both $f_{\min}$ and the lowest threshold value $U_c(f_{\min})$ increase.

Samples of the nematic Phase 4 have also been investigated at $T=30$ °C. Measurements on the frequency dependence of U_c are shown in Fig. 10 for a $d=3.2$ μm cell (circles). At dc voltage (solid triangle) and at low frequencies (up to $f=15$ Hz) flexoelectric domains [see in Fig. 11(a)] have been observed with a tendency of U_f increasing with the frequency. At $f=15$ Hz the thresholds for flexoelectric domains and for traveling dielectric oblique rolls almost coincide [see the coexisting patterns in Fig. 11(b)—a similar behavior has also been reported in [56]]. At higher f flexoelectric domains could not be detected. Instead, traveling dielectric oblique rolls [Fig. 11(c)] or traveling dielectric normal rolls have been observed. The threshold curve for these

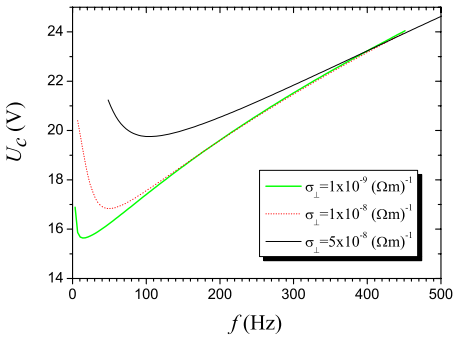

FIG. 9. (Color online) Results of numerical calculations for Phase 5 with $\sigma_a/\sigma_\perp=0.1$, $e_1=-26.5$ pC/m, $e_3=-23.6$ pC/m, and $d=3.4$ μm for three different conductivities $\sigma_\perp$.

traveling rolls has a minimum similar to that observed in dielectric s-EC of Phase 5. In contrast to the thin cell, however, experimental data obtained on a $d=12.4$-μm-thick sample of Phase 4 (star symbols in Fig. 10 and in its inset) demonstrate a monotonically increasing $U_c(f)$ (at least for $f \geqslant 10$ Hz). At the same time, Fig. 10 represents an experimental support of numerical results shown in Fig. 8 obtained though, with Phase 5 parameters (unfortunately, in Phase 5 samples with $d \geqslant 10$ μm, dielectric s-EC could not be obtained at low enough f).

V. NONSTANDARD EC

Previous measurements have shown that in samples of **8**/**7** with typical thickness ($d \geqslant 10$ μm), ns-EC takes place in the whole investigated frequency range at $T \leqslant 85$ °C, characterized by a linear $U_c(f)$ dependence. In the temperature range 85 °C$<T<$90 °C both ns-EC and s-EC could be observed depending on f and d, while above $T=90$ °C s-EC has always appeared at onset [18].

In accordance with the above experimental findings, in our $d=3.4$ μm sample of **8**/**7** ns-EC has been found below

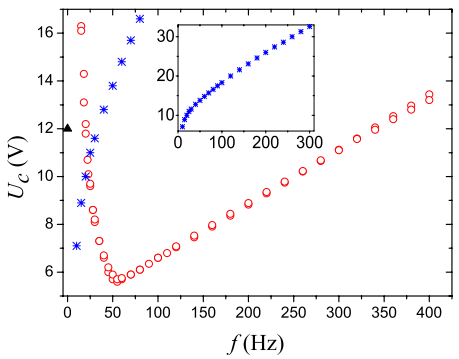

FIG. 10. (Color online) Frequency dependence of the s-EC threshold voltage U_c measured in a sample of Phase 4 with $d=3.2$ μm (circles). At dc voltage, the threshold for the flexoelectric domains is also indicated (solid triangle). For comparison, experimental data obtained on another sample of Phase 4 with $d=12.4$ μm is also plotted (stars). The inset displays experimental results on the $d=12.4$ μm cell in the whole frequency range studied.

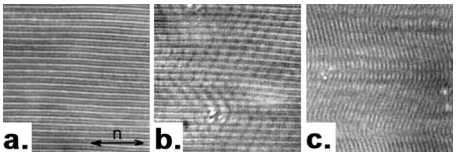

FIG. 11. Snapshots of patterns taken slightly above the threshold in a $d=3.2$ μm sample of Phase 4. (a) Flexoelectric domains at dc voltage. (b) Coexisting flexoelectric domains and traveling dielectric oblique rolls at $f=15$ Hz. (c) Traveling dielectric oblique rolls at $f=70$ Hz. The arrow denotes the initial director. The physical size of the images is (65×65) μm^2.

$T \approx 90$ °C. At higher frequencies, similarly to thick cells, a linear frequency dependence of the threshold voltage has been detected which is illustrated in Fig. 12 for three different temperatures. However, at lower f the frequency dependence of U_c is different from the one observed in thicker samples [18]. The threshold voltage increases abruptly here when $f \to 0$ as shown in Fig. 12; i.e., $U_c(f)$ becomes a nonmonotonic function with a minimum $U_{c\,\mathrm{min}}$ at f_{min}, similarly to the case of dielectric s-EC in Phase 5 and Phase 4 samples.

Studies on the temperature dependence of $U_c(f)$ in the sample of **8**/**7** with $d=3.4$ μm have revealed that (i) $U_{c\,\mathrm{min}}$ reduces with the increase of T; (ii) f_{min} increases with T; (iii) the steepness of $U_c(f)$ in the high frequency range (where the function is linear) is also temperature dependent; dU_c/df diminishes linearly with the increase of T.

In an even thinner ($d=2.4$ μm) sample of **8**/**7** no periodic EC structure could be observed; instead, a large-scale, nonperiodic pattern has appeared at a critical voltage U_{ls}. Since a similar nonperiodic, large-scale pattern has also been observed as a concomitant phenomenon of the ns-EC pattern at U_c in thicker samples, in Fig. 13 we compare this U_{ls} with U_c of ns-EC measured in samples of different thicknesses at $T=76$ °C. It is seen that the nonmonotonic behavior is restricted to the two smallest thicknesses ($d=2.4$ μm and $d=3.4$ μm). f_{min} increases as d is lowered (it is about 220 Hz for the $d=3.4$ μm sample, and is roughly 500 Hz for $d=2.4$ μm). Therefore, one can conclude that f_{min} depends stronger on d, than on the material parameters (compare with

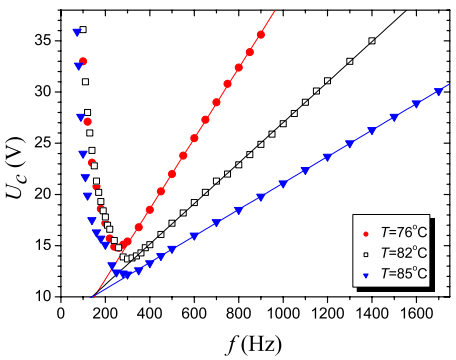

FIG. 12. (Color online) Frequency dependence of the ns-EC threshold voltage U_c measured in a sample of **8**/**7** with $d=3.4$ μm for three different temperatures T. Solid lines represent linear fit to data at high frequencies (above the minima of the curves).

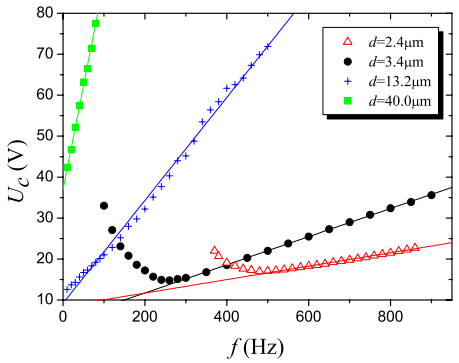

FIG. 13. (Color online) ns-EC threshold curves $U_c(f)$ measured in samples of **8**/**7** of different thicknesses d at $T=76$ °C. Solid lines represent linear fit to data.

the much weaker temperature dependence of this minimum in Fig. 12). It can be noted that while $U_{c\,\mathrm{min}}$ and f_{min} grow, dU_c/df decreases with lowering the sample thickness d.

The temperature range where ns-EC is observable extends to higher T in thin samples compared to thicker ones. To demonstrate this, we plotted in Fig. 14 the frequency dependence of the threshold voltage at $T\approx 90$ °C for three different sample thicknesses. In the thick, $d=40$ μm cell s-EC exists in the whole accessible frequency range. At an intermediate thickness of 13.2 μm a s-EC to ns-EC transition has been observed at $f\approx 500$Hz. In the thin, $d=3.4$ μm cell ns-EC has been detected in the whole frequency range. In this latter case a nonmonotonic $U_c(f)$ is observed, just as at lower temperatures, or in the dielectric s-EC of Phase 5 and Phase 4. Figure 14 demonstrates that a s-EC to ns-EC transition can also be induced by reducing the sample thickness (while keeping the temperature and frequency fixed), in addition to the already reported temperature, frequency, and electric field induced transitions [18].

Recent theoretical advances (the analysis of the extended SM) have shown that the flexoelectric charge separation mechanism could be responsible for the occurrence of ns-EC [11]. Numerical simulations based on the extended SM could actually yield a good agreement with experimental results on

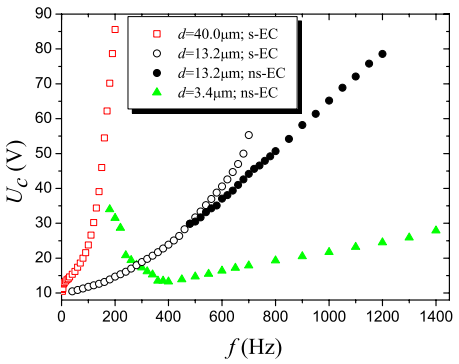

FIG. 14. (Color online) Frequency dependence of the threshold voltage U_c measured in **8**/**7** samples of different thickness ($d=3.4$ μm, 13.2 μm, and 40 μm) at $T\approx 90$ °C (in the vicinity of the s-EC to ns-EC transition). Open symbols denote the s-EC threshold, while closed symbols stand for ns-EC.

a thick sample of the compound **8**/**7** using a reasonable guess for unknown material parameters. Extension of the numerical analysis to smaller thicknesses and lower frequencies is, however, not so straightforward in the parameter range of ns-EC as for s-EC. In addition some important parameters (e.g., viscosities and flexoelectric coefficients) should first be determined by independent measurements. As a consequence a theoretical $U_c(f)$ dependence for Fig. 14 could not yet be provided; it remains a target for further studies.

VI. DISCUSSION

We have reported about measurements of the threshold voltage of electroconvection patterns in various nematic liquid crystals focusing mainly on thin ($d\approx 3.1-3.5$ μm) samples in which $1/\tau_d$ is relatively large. These samples have exhibited patterns of various types in the vicinity of $1/\tau_d$: conductive s-EC, dielectric s-EC as well as nonstandard EC. For all compounds and pattern types we have found an unexpected frequency dependence of the threshold voltage at low frequencies. This indicates that this phenomenon is quite robust. The character of the unusual $U_c(f)$ behavior seems, however, to depend on the type of the pattern. On the one hand, whenever conductive s-EC develop at onset, $U_c(f)$ expresses a pronounced decrease (bending down) if the frequency is lowered, thus $U_c(f)$ has an inflection point. On the other hand, if the onset pattern is dielectric s-EC in the vicinity of $1/\tau_d$, $U_c(f)$ exhibits an abrupt increase (bending up) towards lower f, so $U_c(f)$ has a minimum. In case of ns-EC, the low frequency behavior is similar to that of the dielectric s-EC. As according to recent theoretical results the ns-EC is actually a dielectric mode [11], one can conclude that whether $U_c(f)$ bends down or up at $f\to 0$, depends on the spatiotemporal symmetry of the solution at onset. The significant changes in the curvature of $U_c(f)$ occur in the frequency range of $1/\tau_d$, even though some characteristic frequencies (f_{infl} for the conductive or f_{min} for the dielectric pattern) do not scale precisely with τ_d.

The threshold voltages have also been calculated numerically for s-EC in a linear stability analysis using both the standard model of electroconvection (neglecting flexoelectricity), and the extended SM (including the flexoelectric effect). The simulations have shown that in the absence of flexoelectricity thin as well as thick cells exhibit the "regular" $U_c(f)$ behavior, without the unusual dependence at low f. Including, however, flexoelectricity with properly adjusted flexoelectric coefficients the pronounced low frequency decrease of the conductive s-EC threshold could be reproduced in a quantitative agreement with the experimental data.

Unfortunately, a similar quantitative match could not be achieved for dielectric s-EC patterns. Nevertheless, simulation experiments have shown that even the abrupt increase of the dielectric $U_c(f)$ in thin cells at low f can be qualitatively reproduced by the extended SM if one uses (together with the same flexoelectric coefficients as for the conductive s-EC) a $\sigma_a/\sigma_\perp$ value which is lower than expected from the measurements. One has to emphasize here that the fitted e_1 and e_3 parameters fall into the range of values measured for nematics, however, we do not claim that the fitted values are

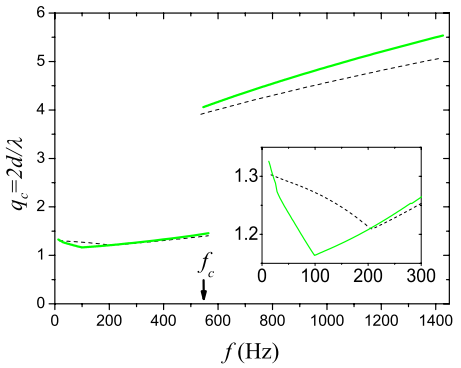

FIG. 15. (Color online) Frequency dependence of the dimensionless critical wave number q_c for Phase 5 with $d=(3.4\pm0.5)$ μm. The solid and the dashed lines are the results of the numerical analysis with and without the flexoelectric effect, respectively. The inset is the magnification of the low frequency range. The arrow indicates the crossover frequency f_c.

unique; some other e_1, e_3 combinations might provide almost as good a match with experimental data. Furthermore, in the numerical calculations only a subset of parameters $(\sigma_a, \sigma_\perp, e_1, e_3)$ have been varied. One cannot exclude that by slight adjustment of the other parameters (allowed by experimental errors in measuring the values in Table I) a better agreement between measurements and calculations could be obtained.

It has already been mentioned in the Introduction that only the sum and the difference of e_1 and e_3 enter the equations of the extended SM. On the one hand, the sum e_1+e_3 provides an additional flexoelectric contribution to the charge density, as seen from the charge conservation equation [Eq. (A11) of Ref. [11]]. On the other hand, the flexoelectric polarization also contributes to the electric torque on the director and by that, both e_1+e_3 and e_1-e_3 enter the equations for the "out-of-plane" (parallel with substrates) and the "in-plane" (perpendicular to substrates) director perturbations [Eqs. (A7) and (A6) of Ref. [11], respectively]. Via coupling of the equations the torque induced director changes modify, however, even the Coulomb charge density. Thus, the influence of the sum and of the difference of flexoelectric coefficients on the onset voltage cannot be clearly separated.

The numerical simulations presented above have confirmed that the experimentally detected low frequency dependencies of $U_c(f)$ are consequences of the flexoelectricity and represent a competition between flexoelectric and Coulomb charge separation mechanisms. The frequency range in which it occurs is in the order of $1/\tau_d$, thus it can be tuned by the proper choice of the sample thickness d.

In the paper we have focused on the EC threshold voltages only. For a complete analysis of the onset behavior one should also address the critical wave vector $\mathbf{q}_c$ of the pattern. In Fig. 15 the simulated $q_c(f)$ curves are presented for the same parameter set as U_c is exhibited in Fig. 1. One can see that in the conductive regime the frequency dependence of q_c is weak and is only slightly affected by flexoelectricity. However, it shifts the Lifshitz point [seen as a kink on the $q_c(f)$ curve in the inset of Fig. 15] considerably. The direction of the shift depends on the material parameter set; for Phase 5 the Lifshitz point moves toward lower f when adding flexoelectricity, while it goes to higher f for MBBA. No additional change of q_c occurs at low f in the frequency range of the U_c bending down. On the other hand, flexoelectricity changes considerably the dielectric $q_c(f)$ and also converts the dielectric rolls from normal to oblique. Interestingly, while flexoelectricity increases q_c, in the same time it decreases the dielectric threshold (see Fig. 1). The special experimental conditions, namely, the fast traveling speed, the related nonuniformity of the rolls, and the relatively weak contrast (weaker than in thick samples) unfortunately did not allow one to obtain $\mathbf{q}_c$ values with required precision by polarizing microscopy, so experimental and theoretical data could not be confronted in the full frequency range.

From the simulation results of the dielectric thresholds presented in Fig. 6 one can draw a double conclusion. On the one hand, the obtained qualitative agreement may indicate that the extended SM does contain the main ingredients of the physical mechanism responsible for the formation of dielectric patterns even under our experimental conditions. On the other hand, however, the lack of quantitative match implies that the applicability limits of the model could be approached by testing thin cells at low frequencies and inclusion of additional phenomena (resulting in an apparent reduction of $\sigma_a/\sigma_\perp$) would be needed for a complete description. One such candidate could be the (unipolar) charge injection at the electrodes which is not included in the SM. It has been suggested recently [57] that for a low value of the overall conductivity (as in our case for dielectric s-EC) the weak charge focusing effect may be disrupted by charge injection at dc or at low frequency ac fields.

At low $\sigma_\perp$ other effects related to the ionic nature of the electrical conductivity may become important. This is emphasized by the fact that in our thin samples for all compounds traveling EC rolls have been detected at the onset. It has been proven that traveling waves can be explained if the assumption of Ohmic conductivity is given up and the SM is replaced by the weak electrolyte model (WEM) [58] taking into account ionic phenomena. It has also been shown that for typical EC samples ($d\gtrsim 10$ μm) in the conductive s-EC regime the U_c and $\mathbf{q}_c$ values provided by the WEM differ by less than 1% from those calculated with the SM [36]. However, in this comparison flexoelectricity has not been included. Neither has the test been performed for smaller d values, nor for dielectric s-EC. Therefore, a more complete description of the observed phenomena would need the inclusion of the flexoelectric effect into the WEM, and an extension of WEM based numerical studies to dielectric s-EC as well as to ns-EC, which is going far beyond the scope of the present paper. Such simulations would require some knowledge about additional material parameters, such as ionic mobility, recombination rate, and equilibrium ion density. In this respect the measurements of the dc and low frequency ac conductivities of thin nematic layers could be important to clarify the impact of weak electrolyte effects. Future studies in these directions could possibly bridge the quantitative gap between the experiments and numerical data presented in this paper for the dielectric s-EC.

ACKNOWLEDGMENTS

The authors thank W. Pesch for fruitful discussions and for providing the numerical code. The authors are grateful to G. Pelzl for providing the liquid crystal **8**/**7**. Financial support by the Hungarian Research Fund Grant No. OTKA-K61075, and DFG Grants No. Kr690/22-1 and No. SFB 481/A8 are gratefully acknowledged.

[1] L. Kramer and W. Pesch, in *Pattern Formation in Liquid Crystals*, edited by Á. Buka and L. Kramer (Springer-Verlag, New York, 1996), p. 221.
[2] L. Kramer and W. Pesch, in *Physical Properties of Liquid Crystals: Nematics*, edited by D. A. Dunmur, A. Fukuda, and G. R. Luckhurst (Inspec, London, 2001), p. 441.
[3] Á. Buka, N. Éber, W. Pesch, and L. Kramer, in *Self Assembly, Pattern Formation and Growth Phenomena in Nano-Systems*, edited by A. A. Golovin and A. A. Nepomnyaschy (Kluwer Academic Press, New York, 2006), p. 55.
[4] E. F. Carr, Mol. Cryst. Liq. Cryst. **7**, 253 (1969).
[5] W. Helfrich, J. Chem. Phys. **51**, 4092 (1969).
[6] S. Rasenat, G. Hartung, B. L. Winkler, and I. Rehberg, Exp. Fluids **7**, 412 (1989).
[7] E. Dubois-Violette and P. Manneville, in *Pattern Formation in Liquid Crystals*, edited by Á. Buka and L. Kramer (Springer-Verlag, New York, 1996), p. 91.
[8] E. Bodenschatz, W. Zimmermann, and L. Kramer, J. Phys. (France) **49**, 1875 (1988).
[9] W. Zimmermann, in *Defects, Singularities and Patterns in Nematic Liquid Crystals*, edited by J. M. Coron, J. M. Ghidaglia, and F. Helein, NATO Advanced Study Institute Series (Kluwer, Dordrecht, 1991), p. 401.
[10] B. Dressel, Ph.D. thesis, University of Bayreuth, 2002.
[11] A. P. Krekhov, W. Pesch, N. Éber, T. Tóth-Katona, and Á. Buka, Phys. Rev. E **77**, 021705 (2008).
[12] S. Rasenat, V. Steinberg, and I. Rehberg, Phys. Rev. A **42**, 5998 (1990).
[13] U. Schneider, M. de la Torre Juarez, W. Zimmermann, and I. Rehberg, Phys. Rev. A **46**, 1009 (1992).
[14] P. G. de Gennes and J. Prost, *The Physics of Liquid Crystals* (Clarendon Press, Oxford, 1993).
[15] M. Goscianski and L. Léger, J. Phys. (France) **36**, 231 (1975).
[16] L. M. Blinov, M. I. Barnik, V. T. Lazareva, and A. N. Trufanov, J. Phys. (France) **40**, 263 (1979).
[17] E. Kochowska, S. Németh, G. Pelzl, and Á. Buka, Phys. Rev. E **70**, 011711 (2004).
[18] T. Tóth-Katona, A. Cauquil-Vergnes, N. Éber, and Á. Buka, Phys. Rev. E **75**, 066210 (2007).
[19] P. Kumar, S. N. Patil, U. S. Hiremath, and K. S. Krishnamurthy, J. Phys. Chem. B **111**, 8792 (2007).
[20] D. Wiant, J. T. Gleeson, N. Éber, K. Fodor-Csorba, A. Jákli, and T. Tóth-Katona, Phys. Rev. E **72**, 041712 (2005).
[21] M.-G. Tamba, W. Weissflog, A. Eremin, J. Heuer, and R. Stannarius, Eur. Phys. J. E **22**, 85 (2007).
[22] R. Stannarius and J. Heuer, Eur. Phys. J. E **24**, 27 (2007).
[23] J. Harden, B. Mbanga, N. Éber, K. Fodor-Csorba, S. Sprunt, J. T. Gleeson, and A. Jákli, Phys. Rev. Lett. **97**, 157802 (2006).
[24] R. B. Meyer, Phys. Rev. Lett. **22**, 918 (1969).
[25] S. Chandrasekhar, *Liquid Crystals* (University Press, Cambridge, 1992).
[26] I. G. Chistyakov and L. K. Vistin, Sov. Phys. Crystallogr. **19**, 119 (1974).
[27] Yu. P. Bobylev and S. A. Pikin, Sov. Phys. JETP **45**, 195 (1977).
[28] M. I. Barnik, L. M. Blinov, A. N. Trufanov, and B. A. Umanski, Sov. Phys. JETP **46**, 1016 (1977).
[29] L. Kramer, E. Bodenschatz, W. Pesch, W. Thom, and W. Zimmermann, Liq. Cryst. **5**, 699 (1989).
[30] W. Thom, W. Zimmermann, and L. Kramer, Liq. Cryst. **4**, 309 (1989).
[31] N. V. Madhusudana and V. A. Raghunathan, Liq. Cryst. **5**, 1789 (1989).
[32] Here, we kept the notations for different modes as introduced in Ref. [11], where the full description of the model is given. In Ref. [9] notations of IA, IIA, IB, and IIB have been used for modes I, II, III, and IV, respectively.
[33] A. P. Krekhov and W. Pesch (unpublished).
[34] H. Kresse, A. Wiegeleben, and D. Demus, Krist. Tech. **15**, 341 (1980).
[35] R. M. Clever and F. H. Busse, J. Fluid Mech. **65**, 625 (1974).
[36] M. Treiber, N. Éber, Á. Buka, and L. Kramer, J. Phys. II **7**, 649 (1997).
[37] A. Hertrich, W. Decker, W. Pesch, and L. Kramer, J. Phys. II **2**, 1915 (1992).
[38] S.-Q. Zhou, N. Éber, Á. Buka, W. Pesch, and G. Ahlers, Phys. Rev. E **74**, 046211 (2006).
[39] Data sheet "N5 Licrystal" from Merck, Darmstadt, Germany, 1982.
[40] H. H. Graf, H. Kneppe, and F. Schneider, Mol. Phys. **77**, 521 (1992).
[41] W. H. de Jeu, W. A. P. Claasen, and A. M. J. Spruijt, Mol. Cryst. Liq. Cryst. **37**, 269 (1976).
[42] F. Rondelez, D. Diguet, and G. Durand, Mol. Cryst. Liq. Cryst. **15**, 183 (1971).
[43] G. J. Sprokel, Mol. Cryst. Liq. Cryst. **22**, 249 (1973).
[44] E. J. Sinclair and E. F. Carr, Mol. Cryst. Liq. Cryst. **37**, 303 (1976).
[45] H. Kneppe, F. Schneider, and N. K. Sharma, J. Chem. Phys. **77**, 3203 (1982).
[46] C. Gähwiller, Phys. Lett. **36**, 311 (1971).
[47] L. M. Blinov, L. A. Beresnev, S. A. Davydyan, S. G. Kononov, and S. V. Yablonski, Ferroelectrics **84**, 365 (1988).
[48] T. Takahashi, S. Hashidate, H. Nishijou, M. Usui, M. Kimura, and T. Akahane, Jpn. J. Appl. Phys., Part 1 **37**, 1865 (1998).
[49] I. Dozov, Ph. Martinot-Lagarde, and G. Durand, J. Phys. (France) Lett. **43**, L–365 (1982).
[50] A. G. Petrov, in *Physical Properties of Liquid Crystals: Nematics*, edited by D. A. Dunmur, A. Fukuda, and G. R. Luckhurts (Inspec, London, 2001), p. 251.
[51] N. Éber, S. A. Rozanski, S. Németh, Á. Buka, W. Pesch, and L. Kramer, Phys. Rev. E **70**, 061706 (2004).

[52] W. Pesch, L. Kramer, N. Éber, and Á. Buka, Phys. Rev. E **73**, 061705 (2006).

[53] Y. Marinov, J. Kosmopoulos, W. Weissflog, A. G. Petrov, and D. J. Photinos, Mol. Cryst. Liq. Cryst. Sci. Technol., Sect. A **357**, 221 (2001).

[54] O. A. Scaldin, A. N. Lachinov, and A. N. Chuvyrov, Sov. Phys. Solid State **27**, 734 (1985).

[55] O. A. Scaldin and A. N. Chuvyrov, Sov. Phys. Crystallogr. **35**, 505 (1990).

[56] Experimental results on a Phase 4 sample with $d \approx 11$ μm—see M. May, W. Schöpf, and I. Rehberg, *Presentation at 35th Topical Meeting on Liquid Crystals*, Bayreuth, Book of Abstracts, 2007, p. P38; http://lc-tagung.uni-bayreuth.de/book_of_abstracts_lc_meeting_2007.pdf

[57] K. S. Krishnamurthy and P. Kumar, Phys. Rev. E **76**, 051705 (2007).

[58] M. Treiber and L. Kramer, Mol. Cryst. Liq. Cryst. Sci. Technol., Sect. A **262**, 311 (1995).